Letter

Double explosive Kuramoto transition in hypergraphs

Sangita Dutta,[1,*] Prosenjit Kundu,[2] Pitambar Khanra,[3] Ludovico Minati,[4,5,†] Stefano Boccaletti,[6,7,8] Pinaki Pal,[1,‡] and Chittaranjan Hens[9]

[1]*Department of Mathematics, National Institute of Technology, Durgapur 713209, India*
[2]*Dhirubhai Ambani Institute of Information and Communication Technology, Gandhinagar, Gujarat 382007, India*
[3]*Department of Chemical and Biological Engineering, The State University of New York at Buffalo, Buffalo, New York 14260, USA*
[4]*School of Life Science and Technology, University of Electronic Science and Technology of China, 611731 Chengdu, China*
[5]*Center for Mind/Brain Sciences (CIMeC), University of Trento, I-38123 Trento, Italy*
[6]*Sino-Europe Complexity Science Center, North University of China, 030051 Taiyuan, China*
[7]*Research Institute of Interdisciplinary Intelligent Science, Ningbo University of Technology, 315104 Ningbo, China*
[8]*CNR - Institute of Complex Systems, Via Madonna del Piano 10, I-50019 Sesto Fiorentino, Italy*
[9]*Center for Computational Natural Science and Bioinformatics, International Institute of Informational Technology, Gachibowli, Hyderabad 500032, India*

(Received 30 December 2024; accepted 8 April 2025; published 2 June 2025)

This study aims to develop a generalized concept that will enable double explosive transitions in the forward and backward directions or a combination thereof. We found two essential factors for generating such phase transitions: the use of higher-order (triadic) interactions and the partial adaptation of a global order parameter acting on the triadic coupling. A compromise between the two factors may result in a double explosive transition. To reinforce numerical observations, we employed the Ott-Antonsen ansatz. We observed that for a wide class of hypergraphs, combining two elements can result in a double explosive transition.

DOI: 10.1103/PhysRevResearch.7.L022049

Introduction. Classical network theory states that if a link joins two nodes with a probability p, a continuous percolation process will develop a giant connected component (GCC). An analytically tractable critical p [1,2] constitutes the foundation for such GCC emergence. Later research showed that if a specific product rule is applied at the time of connection, the critical p can be delayed and the transition becomes explosive (Achlioptas processes; two links compete to be added) [3–5]. More complex behavior can also be guaranteed by further alterations to the connection rule; specifically, by using the three-vertex rule, which connects nodes based on their cluster sizes. This enables numerous discontinuous jumps in the arbitrary vicinity of the first continuous jump [6–8].

Nonequilibrium phase transitions are frequently seen in the networks of complex systems such as Kuramoto oscillators. In particular, the synchronization transitions that characterize the path from incoherence to coherence are determined by the coupling configuration and distribution of intrinsic natural frequencies [9–14]. For example, if the natural frequencies and network structure are correlated and the network is highly heterogeneous [15], the transition becomes explosive [16,17]. Another interesting technique for explosive or discontinuous transitions is adapting the coupling with the Kuramoto order parameter [18–23]. Such adaptations are made elegant by the following characteristics: (i) A network specification is not required. (ii) Different types of frequency sets can be operated across.

These two observations—one from networks (stairlike discontinuities) and the other from coupled Kuramoto oscillators (explosive transitions)—motivate the crucial question of whether the strategic creation of a method for producing stairlike (specifically, double-explosive-transition) discontinuities in coupled Kuramoto oscillators is possible. If so, what kind of coupling will it have? Can we move it in only one direction, that is, forward or backward? Stairlike behavior has been observed in the Sakaguchi-Kuramoto model in random networks with partial degree-frequency correlation [24]. Notably, it was also observed in a finite graph of second-order Kuramoto oscillators. Varieties size of clusters coexist in hysteretic regimes when there is considerable inertia [25]. Further, more intricate stairlike behavior was developed in Ref. [26] in the presence of high inertia and in Ref. [27] in the presence of higher-order interactions. A recent study have suggested that if suitable frequency selections are made and the network connection is temporally adjusted, a finite network of Kuramoto oscillators may display a stairlike discontinuous transition [28]. Most recently, a double hysteresis loop in duplex networks with a high phase-lag has been quantitatively detected [29]. However, to date, no universal mechanism or technique has been developed to realize a double hysteresis loop or

*Contact author: sangitaduttaprl@gmail.com
†Contact author: lminati@uestc.edu.cn; lminati@ieee.org
‡Contact author: ppal.maths@nitdgp.ac.in

explosive transition (with Kuramoto oscillators) in a single direction.

In this Letter, we propose a broad approach that can produce a double explosive transition in one or both directions. Our method utilizes two key factors: (i) We employed hypergraphs to account for pairwise and triadic interactions [30,31]. (ii) Building on previous research [18], we suggest a partial adaptation of the order parameter. The first factor guarantees tiered or explosive synchronization with or without adaptation [32–40]. The second factor enables control of the explosion width [18] without the need to consider any particular networks or frequencies. We have observed multiple nontrivial incoherence to coherence transitions in a hypergraph of Kuramoto oscillators when both factors were combined. Based on the Ott-Antonsen ansatz [41], for a hypergraph, we have established that a partial adaptation can be used to increase or decrease the size of double explosive loops (for a given higher-order interaction strength). Evidence suggests that such double loops may be removed and a single stair can appear in either direction with careful adaptation. Ultimately, using average-frequency analysis, we demonstrate how the dyadic coupling strength—or the adaptation in triadic coupling—influences the development or decline of the clusters.

The coupled Kuramoto model can be expressed as

$$\dot{\theta}_i = \omega_i + K_1 r_1^a \sum_{j=1}^{N} A_{ij} \sin(\theta_j - \theta_i - \beta) + K_2 r_1^b \sum_{j=1}^{N}\sum_{k=1}^{N} B_{ijk} \sin(2\theta_j - \theta_k - \theta_i - \beta), \quad i = 1, 2, \ldots, N, \tag{1}$$

where A_{ij} is the ijth element of the adjacency matrix A wherein $A_{ij} = 1$ if there is a pairwise connection between the ith and jth node, otherwise $A_{ij} = 0$; similarly, B_{ijk} represents the triangular connections between the three nodes i, j, and k, wherein $B_{ijk} = 1$ if the three nodes form a triangle, otherwise 0; ω_i is the natural frequency drawn from the Lorentzian distribution $g(\omega) = \frac{\Delta}{\pi[\Delta^2 + (\omega - \omega_0^2)]}$, wherein Δ is the half width at half maximum and ω_0 is the center of the distribution. N is the total number of oscillators in the system and the nonzero a and b control the strength of adaptation in pairwise coupling (K_1) and higher-order coupling (K_2), respectively. β indicates the phase frustration or phase-lag of the system [42,43]. We did not investigate the role of β in this study; however, it has been used in the analytical computation. Given that β suppresses synchronization [36,37,43,44], conducting a separate study to determine how to create and destroy double or stairlike explosive synchronization considering β is necessary. For the construction of hypergraphs, please see Supplemental Material Sec. II [45]. To proceed further, let us first define the order parameters, which characterize the synchronization level. The local order parameters are defined as $R_i^1 = \sum_{j=1}^{N} A_{ij} e^{i\theta_j}$ and $R_i^2 = \sum_{j,k=1}^{N} B_{ijk} e^{2i\theta_j} e^{-i\theta_k}$, and the global order parameters can be defined as [46] $z_1 = r_1(t) e^{i\psi_1} = \frac{1}{N\langle k^{(1)}\rangle} \sum_{i=1}^{N} R_i^1$ and $z_2 = r_2(t) e^{i\psi_2} = \frac{1}{2N\langle k^{(2)}\rangle} \sum_{i=1}^{N} R_i^2$, where $\langle k^{(1)}\rangle$ and $\langle k^{(2)}\rangle$ denote the mean pairwise and triadic degrees, respectively, and ψ_1 and ψ_2 are the average phase values. In this study, the global order parameter r_1 was modified to consider both coupling strengths in the form of $K_1 r_1^a$ and $K_2 r_1^b$.

Further calculations using the Ott-Antonsen ansatz [41,46] give the reduced order model (see Supplemental Material Sec. III [45]):

$$\dot{\alpha} + i\omega_0\alpha + \Delta\alpha - \frac{K_1 r_1^a}{2} \sum_{k'} N(k') p^{(2)}(k,k')[\alpha(k') e^{i\beta} - \bar{\alpha}(k')\alpha^2(k) e^{-i\beta}] - \frac{K_2 r_1^b}{2} \sum_{k',k''} N(k')N(k'') p^{(3)}(k,k',k'') \times [\alpha^2(k')\bar{\alpha}(k'') e^{i\beta} - \bar{\alpha}^2(k')\alpha(k'')\alpha^2(k) e^{-i\beta}] = 0. \tag{2}$$

The global order parameters can be calculated as

$$z_1(t) = \frac{1}{N\langle k^{(1)}\rangle} \sum_{k,k'} N(k)N(k') p^{(2)}(k,k') \times \bar{\alpha}(\omega_0 - i\Delta, k', t), \tag{3}$$

$$z_2(t) = \frac{1}{2N\langle k^{(2)}\rangle} \sum_{k,k',k''} N(k)N(k')N(k'') p^{(3)}(k,k',k'') \times \bar{\alpha}^2(\omega_0 - i\Delta, k', t)\alpha(\omega_0 - i\Delta, k'', t), \tag{4}$$

where $p^{(2)}$, $p^{(3)}$ are the link and triangle connection probabilities, respectively, k, k' are node degrees, $N(k)$ is the number of nodes having degree k, α is the coefficient in the Fourier series of the density function of the considered system, and $\bar{\alpha}$ is its conjugate. Solving Eqs. (2)–(4) gives the synchronization profiles for different network topologies. Now, we will examine how the global order parameter r_1 is affected by the adaptive parameters (a, and b), adaptation, and the higher-order coupling K_2, beginning with degree-correlated networks.

Degree-correlated networks. In this section, we examine the case where the network (hypergraph) is generated based on prescribed node degrees. For this purpose, we take a degree sequence $\{k_1, k_2, \ldots, k_N\}$ and create links with probability $p^{(2)}(k,k') = \frac{kk'}{N\langle k^{(1)}\rangle}$ and triangles with probability $p^{(3)}(k,k',k'') = \frac{2kk'k''}{(N\langle k^{(2)}\rangle)^2}$ [31]. Note that here we have taken $\langle k^{(1)}\rangle = \langle k^{(2)}\rangle = \langle k\rangle$. Using the same theoretical analysis, we can elucidate the behavior of the generated network under order-parameter adaptation (see Supplemental Material Sec. IV [45] for detailed calculations). Inserting the probabilities $p^{(2)}$ and $p^{(3)}$ into Eq. (2) gives the self-consistent equations in terms of U_1 and U_2,

$$U_1 = \sum_k \frac{kN(k)\alpha(k, U_1, U_2)}{N\langle k\rangle}, \tag{5}$$

$$U_2 = \sum_k \frac{kN(k)\alpha^2(k, U_1, U_2)}{N\langle k\rangle} \tag{6}$$

where

$$\alpha = \frac{-1 + \sqrt{1 + \left(K_1 r_1^a k U_1 + 2K_2 r_1^b k U_1 U_2\right)^2 \cos^2\beta}}{\left(K_1 r_1^a k U_1 + 2K_2 r_1^b k U_1 U_2\right)\cos\beta} \tag{7}$$

and $r_1(t) = U_1$. Now we solve the self-consistent Eqs. (5) and (6) to find the order parameter values. Moreover, the

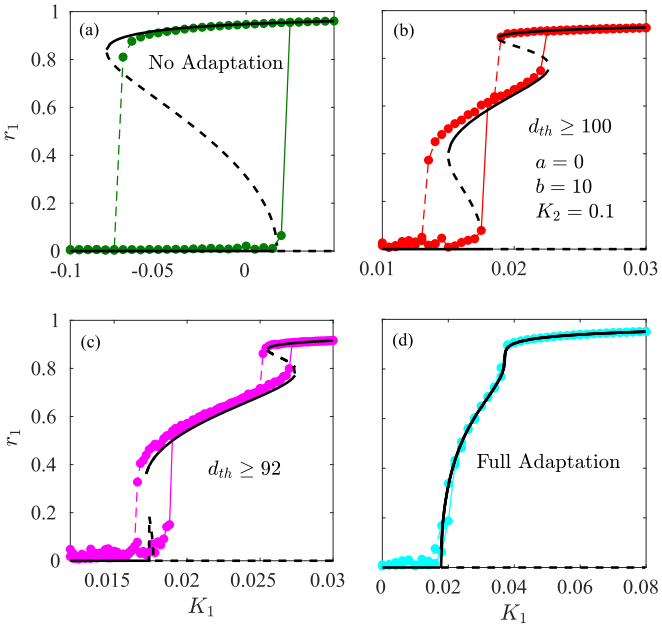

FIG. 1. Synchronization profiles showing r_1 as a function of K_1 for (a) no adaptation, (b) $d_{\text{th}} = 100$, (c) $d_{\text{th}} = 92$, and (d) full adaptation. Black solid and dashed lines indicate stable and unstable solutions of the self-consistent equations, respectively. Colored (green, red, magenta, and cyan) solid circles joined with solid and dashed lines represent numerically simulated data points for the forward and backward directions, respectively. All other parameters were fixed ($a = 0$, $b = 10$, and $K_2 = 0.1$).

relationship between U_1 and U_2 is demonstrated by $U_2 \sim U_1^2$. Finally, the critical coupling strength can be expressed as

$$K_1^c = \frac{2\langle k \rangle}{\langle k^2 \rangle \cos\beta}. \tag{8}$$

The role of β is not being examined in this discussion. Instead, it is the first and second moments of the degree distribution that will influence the onset of synchronization. To validate these analytical findings, we constructed a network with a size of $N = 5000$ using the recommended procedure, in which the degree sequence was drawn from a uniform distribution. A degree-correlated network having power-law degree distribution is analyzed in Supplemental Material Sec. IV B [45].

Uniform distributions. First, we take a degree sequence drawn randomly from a uniform distribution on [75, 145]. Here, the average degrees $\langle k \rangle$ and $\langle k^2 \rangle$ are in the order of 10^2 (109) and 10^4 (12 372), respectively. The phase-lag parameter (β) is fixed at zero. The partial adaptive technique is primarily utilized in the higher-order interaction (HOI) term. We select nodes with degrees greater or equal to a threshold value (d_{th}). The global order parameter r_1 is used in conjunction with the HOI coupling of those nodes (we are using r_1^b to test the effect of b). Figure 1 shows how d_{th} affects the synchronization order parameter r_1. The HOI coupling K_2 is fixed at 0.1 and the other parameters remain constant at $a = 0$, $b = 10$, and $\beta = 0$ in this case. Note that the pairwise component is not adapted when $a = 0$. The combined roles of a and b are discussed in Supplemental Material Sec. IV [45]. The Euler method is used to integrate Eq. (1) for numerical simulation and we have solved the self-consistent Eqs. (5) and (6) to obtain analytical r_1 values. Using a Lorentzian distribution with $\omega_0 = 0$ and half width $\Delta = 1$, the natural frequencies can be extracted. The initial phases of the oscillators are drawn from a uniform distribution $[-\pi, \pi]$. After sufficiently removing the transient parts, we can calculate stationary values of the order parameter r_1 in both the forward and backward directions. Forward simulation begins with the incoherent state at $K_1 = -0.1$ and advances in small increments $\Delta K_1 = 0.0005$ until the strong synchronized state ($K_1 = 0.5$) is reached. Final phase values from each previous solution are utilized to integrate the system, serving as the initial conditions at each coupling strength. Conversely, the backward simulation starts from the synchronized state ($K_1 = 0.5$) and decreases with the same step size as the forward simulation until the incoherent state is reached. Similar to the forward simulation, the final phase values of the previous solution are used as the starting point for each iteration. Figure 1(a) shows the transition of r_1 as a function of K_1 without any adaptation. The path to transition is clearly explosive in this case, which is consistent with previous studies [32,36]. In Fig. 1(b) r_1 was adapted to the nodes having degree greater than or equal to 100 ($d_{\text{th}} = 100$). Here, a new type of synchronization transition scenario is observed. A weak synchronized state facilitates the transition from the incoherent to synchronized state. The solutions to the self-consistent equations show that a stable state emerges between two unstable states. As a result, the system makes two abrupt jumps, one forward and one backward. A decrease in the threshold value (implying more adapted nodes) increases the length of the generated stable state, reducing the width of both hystereses [Fig. 1(c)]. These are the key findings of this study. A carefully chosen subset of adapted nodes in a hypergraph can result in a double hysteresis loop. As more nodes are adapted, the network will eventually follow a classical route, that is, a continuous route to synchronization [Fig. 1(d), with all nodes adapted]. Thus, in the case of partial adaptation $d_{\text{th}} = 100$ and 92, we observe a double hysteresis loop along the transition route. The analytical derivation of the synchronization onset [Eq. (8)] indicates that it is only affected by $\langle k \rangle$ and $\langle k^2 \rangle$. Other parameters cause the system to exhibit nonlinear effects. The K_1^c value of the generated network is 0.0177 for all transitions, which has been numerically verified. In Supplemental Material Sec. IV B [45], we explore the role of the degree threshold value (d_{th}) and triadic coupling K_2 for a network with a power-law degree distribution. The same phenomenon is also observed in the degree-uncorrelated (random) network discussed in Supplemental Material Sec. V [45].

One may wonder whether such an adaptation technique can cause other types of synchronization transitions. For instance, what values of d_{th} and K_2 are suitable for generating tiered synchronization [37,47]. For a given K_2, b, and a, how does the behavior of r_1 change when d_{th} is gradually varied from small (full adaptation) to the highest value (no adaptation)? This scenario is illustrated in Fig. 2, with the combined effects of d_{th} and K_2 shown. We separated the regimes based on different synchronization transition routes obtained from the self-consistent equations. The regimes consist of the following routes to synchronization: Regime

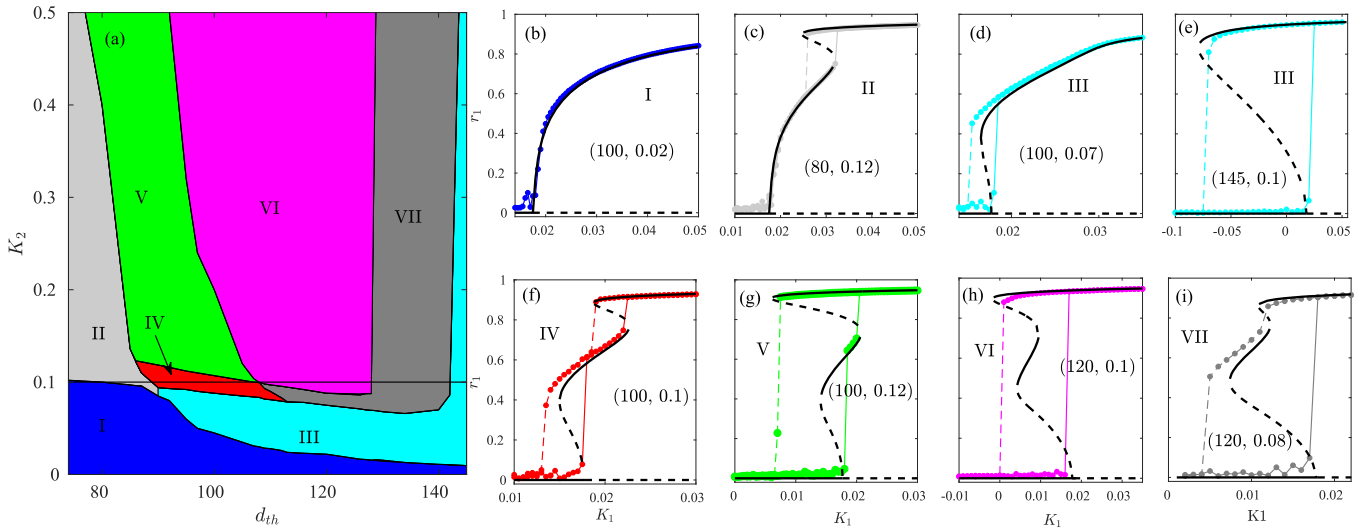

FIG. 2. Bifurcation diagrams. (a) A two-parameter stability diagram in K_2-d_{th} space depicting the different synchronization transition regimes. Blue, gray, cyan, red, light green, magenta, and dark gray present the regimes for continuous, tiered, classical explosive, forward and backward double jump, forward double jump, explosive with stable middle states, and backward double jump synchronization transitions, respectively. (b)–(i) r_1 as a function of K_1 for different parameter-pair values: $(K_2, d_{\text{th}}) = (100, 0.02)$, (80,0.12), (100,0.07), (145,0.1), (100,0.1), (100,0.12), (120,0.1), and (120,0.08), respectively. Black solid and dashed lines indicate stable and unstable solutions of the self-consistent equations, respectively. Numerically simulated data points for forward and backward directions are represented by solid colored circles connected by solid and dashed lines, respectively. The colors of the numerical data points are the same as the regimes in (a). All other parameters were fixed ($a = 0$ and $b = 10$).

I (shaded in blue) represents the continuous route. Due to the weak HOI strength and the adaptation of many nodes (bottom-left corner), pairwise coupling is predominant. This is further confirmed by Fig. 2(b). Regime II (light gray) represents the tiered synchronization occurring at a slightly higher HOI strength. A small, unstable branch can be observed in the upper part of the order parameter [Fig. 2(c)]. Regimes IV–VII are nontrivial, and in all these cases a stable branch appears in the middle ($r_1 \sim 0.6$). The upper ($r_1 \sim 1$) and lower stable branches ($r_1 \sim 0.0$) are connected to the middle branch by two unstable paths. In regime V (green), the system experiences two jumps toward synchronization in the forward direction. However, in the backward direction, it jumps directly to the incoherent state. In contrast, in regime VII (dark gray), the system only makes two jumps in the backward direction. These are further confirmed by Figs. 2(g) and 2(i), respectively. In the intermediate regime VI, the system follows explosive routes [Fig. 2(h)], though there are stable states between the forward and backward transition points. A gradual and adaptive initial phase will not reveal the middle regime; however, a proper choice of initial condition will lead the system to the stable states. In the narrow regime IV (red), the system exhibits double jumps to synchronization in both the forward and backward directions. This is further confirmed in Fig. 2(f). For a lower K_2, an increasing d_{th} (fewer adaptive nodes) leads to explosive synchronization [regime III, cyan, Figs. 2(d) and 2(e)]. A trade-off between adaptive nodes and the HOI strength causes the system to switch from one regime to another. These two parameters contribute to the creation, annihilation, and change of orientation in the middle stable branch. Four points chosen from the black horizontal line in Fig. 2(a) are illustrated in Fig. 1.

Next, we will explore the effect of other parameters, such as a and b. To do this, we will use values of b as 9, 10, 11, and 14 to compare the transition routes reported in Fig. 3.

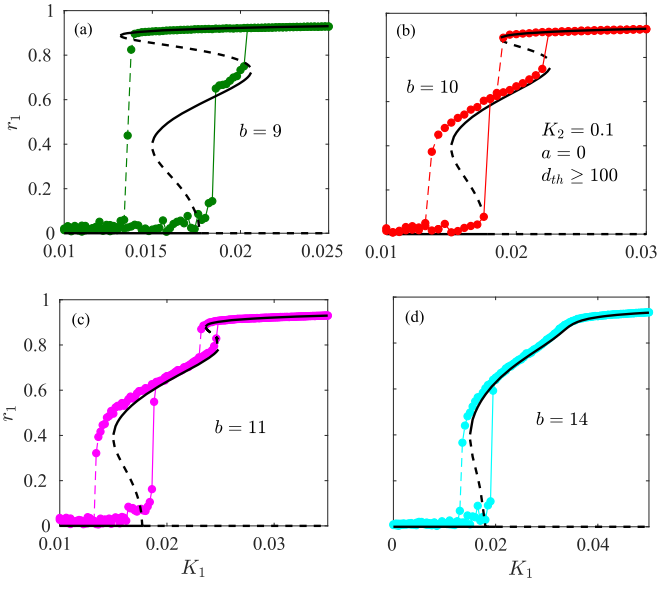

FIG. 3. Synchronization profiles showing r_1 as a function of K_1 for (a) $b = 9$, (b) $b = 10$, (c) $b = 11$, and (d) $b = 14$. Black solid and dashed lines indicate stable and unstable solutions of the self-consistent equations, respectively. Colored (green, red, magenta, and cyan) solid circles joined with solid and dashed lines represent numerically simulated data points for the forward and backward directions, respectively. All other parameters are fixed ($a = 0$, $d_{\text{th}} = 100$, and $K_2 = 0.1$).

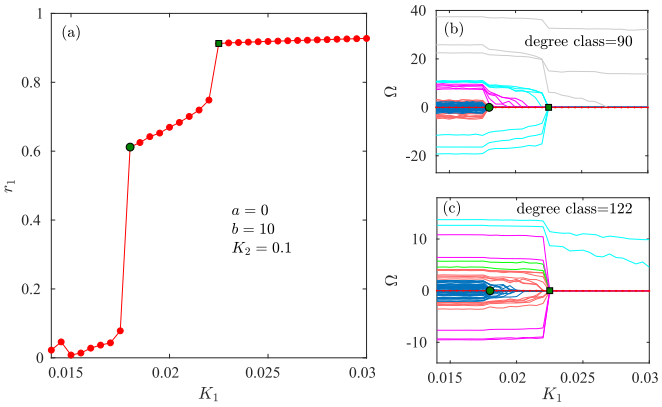

FIG. 4. Frequency evolution of double explosive synchronization transition. (a) r_1 as a function of K_1 for a double jump in the forward simulation. Two transition points are indicated by a solid green circle and square. Mean frequency as a function of K_1 for (b) 90 degree (not adapted) and (c) 122 degree (adapted) classes. The blue, light red, light green, magenta, cyan, and gray colors represent nodes with natural frequencies in the ranges $|\omega_i| < 2$, (2, 4), (4,6), (6, 10), (10, 20), and >20, respectively. The dotted red line represents the mean frequency of the network.

The other parameters remain fixed at $d_{\text{th}} = 100$, $K_2 = 0.1$, and $a = 0$. For $b = 9$, the upper hysteresis broadened and the lower hysteresis remained similar to $b = 10$, whereas for $b = 11$ the width of the upper hysteresis shrank and for $b = 14$ it vanished. However, the lower hysteresis remained constant. Therefore, the exponent b affects only the upper part of the hysteresis. The numerical data also support our analysis.

Finally, we will discuss the relevant mechanisms of the double explosive transition. Because of partial adaptation, a new stable branch emerges in the middle of the synchronization transition. This raises the question of which nodes are involved in the synchronization transition on that particular branch. Thus, to visualize the node behavior, we computed the effective frequency, as given by

$$\Omega_i = \frac{1}{T}\int_t^{t+T} \dot{\theta}_i(\tau)d\tau, \tag{9}$$

where T is the total simulation time. Figure 4 depicts the synchronization transition and corresponding effective frequencies at parameter values $K_2 = 0.1$, $a = 0$, $b = 10$, and $d_{\text{th}} = 100$. We adapted the order parameter r_1 to the nodes with degrees greater than the threshold value (d_{th}). Thus, we have shown the evolution of Ω_i for two degree classes—one adapted (122) and another nonadapted (90). The frequencies in Fig. 4 are colored according to the range of their natural frequencies: blue, light red, light green, magenta, cyan, and gray for $|\omega_i| < 2$, (2, 4), (4,6), (6, 10), (10,20), and >20, respectively. The figure clearly demonstrates that, at the two critical points, the frequencies jump abruptly to the average frequency. Figure 4(b) shows that the nonadapted nodes join the synchronized cluster at the first (second) transition point in the range $|\omega_i| < 6$ ($|\omega_i| < 20$) approximately. The adapted nodes whose frequencies are very close to 0 join the synchronized cluster at the first transition point, and adapted nodes with $|\omega_i| < 10$ join at the second transition point [Fig. 4(c)]. Subsequently, the remaining nodes with frequencies $|\omega_i| > 10$ join one by one as the coupling strength increases. This occurs due to the order parameter adaptation, which reduces the effective coupling strength. Similarly, we have computed the frequency Ω for other synchronization transitions (see Supplemental Material Sec. VI [45]). This clarifies the basic mechanisms behind the double jump in the transition paths.

Discussion. In this Letter, a general principle for realizing a double explosive transition in forward, backward, or a combination of both directions was proposed. The use of triadic interactions and the partial adaptation of the global order parameter operating on the triadic coupling can be considered for the creation of such a phase transition. We tested this technique with degree-correlated uniform and power-law graphs. We also observed this phenomenon in uncorrelated random hypergraphs. The critical coupling for the onset of synchronization was also derived. The partial adaptation and the exponents in the adaptation order parameter tune and control the widths of the double explosive transition. In future studies, we will investigate triple explosive transitions in directed hypergraphs.

Acknowledgments. S.D. acknowledges the support from DST, India under the INSPIRE program (Code No. IF190605). L.M. gratefully acknowledges the support of the "Hundred Talents" program of the University of Electronic Science and Technology of China, of the "Outstanding Young Talents Program (Overseas)" program of the National Natural Science Foundation of China, and of the talent programs of the Sichuan province and Chengdu municipality.

Data availability. No data were created or analyzed in this study.

[1] M. Newman, *Networks: An Introduction* (Oxford University Press, Oxford, UK, 2010).
[2] P. Erdős and A. Rényi, On random graphs I, Publ. Math. Debrecen **6**, 290 (1959).
[3] M. Li, R.-R. Liu, L. Lü, M.-B. Hu, S. Xu, and Y.-C. Zhang, Percolation on complex networks: Theory and application, Phys. Rep. **907**, 1 (2021).
[4] D. Achlioptas, R. M. D'Souza, and J. Spencer, Explosive percolation in random networks, Science **323**, 1453 (2009).
[5] O. Riordan and L. Warnke, Explosive percolation is continuous, Science **333**, 322 (2011).
[6] J. Nagler, T. Tiessen, and H. W. Gutch, Continuous percolation with discontinuities, Phys. Rev. X **2**, 031009 (2012).
[7] R. M. D'Souza and J. Nagler, Anomalous critical and supercritical phenomena in explosive percolation, Nat. Phys. **11**, 531 (2015).
[8] O. Riordan and L. Warnke, Achlioptas processes are not always self-averaging, Phys. Rev. E **86**, 011129 (2012).
[9] S. Boccaletti, G. Bianconi, R. Criado, C. I. Del Genio, J. Gómez-Gardenes, M. Romance, I. Sendina-Nadal, Z. Wang, and M. Zanin, The structure and dynamics of multilayer networks, Phys. Rep. **544**, 1 (2014).

[10] F. A Rodrigues, T. K. DM. Peron, P. Ji, and J. Kurths, The Kuramoto model in complex networks, Phys. Rep. **610**, 1 (2016).
[11] Y. Kuramoto, *Chemical Turbulence* (Springer, Berlin, 1984).
[12] P. Kundu, C. Hens, B. Barzel, and P. Pal, Perfect synchronization in networks of phase-frustrated oscillators, Europhys. Lett. **120**, 40002 (2017).
[13] M. Zanin, D. Papo, P. A. Sousa, E. Menasalvas, A. Nicchi, E. Kubik, and S. Boccaletti, Combining complex networks and data mining: why and how, Phys. Rep. **635**, 1 (2016).
[14] T. Ichinomiya, Frequency synchronization in a random oscillator network, Phys. Rev. E **70**, 026116 (2004).
[15] B. C. Coutinho, A. V. Goltsev, S. N. Dorogovtsev, and J. F. F. Mendes, Kuramoto model with frequency-degree correlations on complex networks, Phys. Rev. E **87**, 032106 (2013).
[16] J. Gómez-Gardenes, S. Gómez, A. Arenas, and Y. Moreno, Explosive synchronization transitions in scale-free networks, Phys. Rev. Lett. **106**, 128701 (2011).
[17] T. Qiu, Y. Zhang, J. Liu, H. Bi, S Boccaletti, Z. Liu, and S. Guan, Landau damping effects in the synchronization of conformist and contrarian oscillators, Sci. Rep. **5**, 18235 (2015).
[18] X. Zhang, S. Boccaletti, S. Guan, and Z. Liu, Explosive synchronization in adaptive and multilayer networks, Phys. Rev. Lett. **114**, 038701 (2015).
[19] M. Manoranjani, V. R. Saiprasad, R. Gopal, D. V. Senthilkumar, and V. K. Chandrasekar, Phase transitions in an adaptive network with the global order parameter adaptation, Phys. Rev. E **108**, 044307 (2023).
[20] G. Filatrella, N. F. Pedersen, and K. Wiesenfeld, Generalized coupling in the Kuramoto model, Phys. Rev. E **75**, 017201 (2007).
[21] P. Khanra, P. Kundu, P. Pal, P. Ji, and C. Hens, Amplification of explosive width in complex networks, Chaos **30**, 031101 (2020).
[22] P. Khanra and P. Pal, Explosive synchronization in multilayer networks through partial adaptation, Chaos, Solitons Fractals **143**, 110621 (2021).
[23] D. Biswas and S. Gupta, Effect of adaptation functions and multilayer topology on synchronization, Phys. Rev. E **109**, 024221 (2024).
[24] P. Kundu and P. Pal, Synchronization transition in Sakaguchi-Kuramoto model on complex networks with partial degree-frequency correlation, Chaos **29**, 013123 (2019).
[25] S. Olmi, A. Navas, S. Boccaletti, and A. Torcini, Hysteretic transitions in the Kuramoto model with inertia, Phys. Rev. E **90**, 042905 (2014).
[26] J. Gao and K. Efstathiou, Synchronized clusters in globally connected networks of second-order oscillators: Uncovering the role of inertia, Chaos **31**, 093137 (2021).
[27] A. Carballosa, A. P. Muñuzuri, S. Boccaletti, A. Torcini, and S. Olmi, Cluster states and π-transition in the Kuramoto model with higher order interactions, Chaos, Solitons Fractals **177**, 114197 (2023).
[28] J. Fialkowski, S. Yanchuk, I. M. Sokolov, E. Schöll, G. A. Gottwald, and R. Berner, Heterogeneous nucleation in finite-size adaptive dynamical networks, Phys. Rev. Lett. **130**, 067402 (2023).
[29] A. Seif and M. Zarei, Double hysteresis loop in synchronization transitions of multiplex networks: The role of frequency arrangements and frustration, Chaos, Solitons & Fractals **196**, 116412 (2025).
[30] O. T. Courtney and G. Bianconi, Generalized network structures: The configuration model and the canonical ensemble of simplicial complexes, Phys. Rev. E **93**, 062311 (2016).
[31] N. W. Landry and J. G. Restrepo, The effect of heterogeneity on hypergraph contagion models, Chaos **30**, 103117 (2020).
[32] P. S. Skardal and A. Arenas, Higher order interactions in complex networks of phase oscillators promote abrupt synchronization switching, Commun. Phys. **3**, 218 (2020).
[33] P. S. Skardal and C. Xu, Tiered synchronization in coupled oscillator populations with interaction delays and higher-order interactions, Chaos **32**, 053120 (2022).
[34] A. Suman and S. Jalan, Finite-size effect in Kuramoto oscillators with higher-order interactions, Chaos **34**, 101101 (2024).
[35] S. Dutta, P. Kundu, P. Khanra, C. Hens, and P. Pal, Perfect synchronization in complex networks with higher-order interactions, Phys. Rev. E **108**, 024304 (2023).
[36] S. Dutta, A. Mondal, P. Kundu, P. Khanra, P. Pal, and C. Hens, Impact of phase lag on synchronization in frustrated Kuramoto model with higher-order interactions, Phys. Rev. E **108**, 034208 (2023).
[37] S. Dutta, P. Kundu, P. Khanra, C. Hens, and P. Pal, Transition to synchronization in the adaptive Sakaguchi-Kuramoto model with higher-order interactions, Phys. Rev. E **110**, 064317 (2024).
[38] M. S. Anwar, S. N. Jenifer, P. Muruganandam, D. Ghosh, and T. Carletti, Synchronization in adaptive higher-order networks, Phys. Rev. E **110**, 064305 (2024).
[39] M. S. Anwar, N. Frolov, A. E. Hramov, and D. Ghosh, Self-organized bistability on globally coupled higher-order networks, Phys. Rev. E **109**, 014225 (2024).
[40] R. Ghosh, Md S. Anwar, D. Ghosh, J. Kurths, and M. D. Shrimali, Transitions to synchronization in adaptive multilayer networks with higher-order interactions, arXiv:2501.12301.
[41] E. Ott and T. M. Antonsen, Low dimensional behavior of large systems of globally coupled oscillators, Chaos **18**, 037113 (2008).
[42] H. Sakaguchi and Y. Kuramoto, A soluble active rotater model showing phase transitions via mutual entertainment, Prog. Theor. Phys. **76**, 576 (1986).
[43] P. Kundu, P. Khanra, C. Hens, and P. Pal, Transition to synchrony in degree-frequency correlated Sakaguchi-Kuramoto model, Phys. Rev. E **96**, 052216 (2017).
[44] O. E. Omel'chenko and M. Wolfrum, Nonuniversal transitions to synchrony in the sakaguchi-kuramoto model, Phys. Rev. Lett. **109**, 164101 (2012).
[45] See Supplemental Material at http://link.aps.org/supplemental/10.1103/PhysRevResearch.7.L022049 for the construction of hypergraphs, the derivation and analysis of the self-consistent equations for degree-correlated networks and random network, the synchronization transitions for partial order parameter adaptation with the pairwise coupling, the frequency evolution of nodes during different kinds of synchronization transitions.
[46] S. Adhikari, J. G. Restrepo, and P. S. Skardal, Synchronization of phase oscillators on complex hypergraphs, Chaos **33**, 033116 (2023).
[47] P. Rajwani, A. Suman, and S. Jalan, Tiered synchronization in Kuramoto oscillators with adaptive higher-order interactions, Chaos **33**, 061102 (2023).